Hindawi
Advances in Civil Engineering
Volume 2022, Article ID 9405338, 12 pages
https://doi.org/10.1155/2022/9405338

Research Article

Multiple Reflective Cracks in Semirigid Base Asphalt Pavement under Traffic Load Using XFEM

Lei Guo,[1] **Jinchao Yue**,[1] **Pan Guo**,[2] **and Xiaofeng Wang**[3]

[1]*School of Water Conservancy Engineering, Zhengzhou University, Henan450001, China*
[2]*School of Mechanics and Safety Engineering, Zhengzhou University, Henan 450001, China*
[3]*Henan Provincial, Communications Planning & Design Institute Co., Ltd, Henan450001, China*

Correspondence should be addressed to Pan Guo; panguo@zzu.edu.cn

Received 3 March 2022; Revised 10 May 2022; Accepted 13 May 2022; Published 26 May 2022

Academic Editor: Piotr Smarzewski

Copyright © 2022 Lei Guo et al. This is an open access article distributed under the Creative Commons Attribution License, which permits unrestricted use, distribution, and reproduction in any medium, provided the original work is properly cited.

This paper built a three-dimensional layered structure model of semirigid base asphalt pavement with single and double transverse reflective cracks based on the Extended Finite Element Method and fatigue fracture theory. The effects of the number of cracks, crack spacing, and crack length on the stress intensity factors (KI, KII, and Keff) under moving vehicle loads were studied. The fracture life of the asphalt pavement structure was calculated based on the Pairs formula. The results demonstrate that reflective cracks in semirigid asphalt pavement are composite cracks of type I and type II under moving vehicle loads, and shear fracture is the main reason for the failure of the base. The damage to the pavement base will be accelerated with the increase in the number of cracks and the length of the cracks. As the distance between the two reflection fractures is closer, the interaction between the cracks has a superimposed enhancement effect on the crack propagation. Compared with the single nonpenetrating crack model, the fatigue life of the nonpenetrating reflective crack in the double crack pavement structure with a crack spacing of 30 cm is reduced by 46.87%. The research on the propagation mechanism of reflective cracks in this paper provides the essential theoretical and numerical basis for the design, construction, working condition evaluation, and maintenance of pavement structures.

1. Introduction

Due to the characteristics of solid integrity and high bearing capacity, semirigid base asphalt pavement has become a common pavement structure form of high-grade highways in China. The microcracks, generated during the strength formation process of the cement-stabilized macadam base, are easily aggregated to form macro-cracks and expand under the action of temperature changes, traffic loads, and other factors [1]. At present, the problem of reflective cracks has become one of the primary failure forms of semirigid base asphalt pavement structures and has received extensive attention from scholars.

In recent years, scholars have conducted in-depth research on the generation, expansion, and suppression mechanism of reflective cracks by using the boundary element method [2], meshless method [3], and finite element [4]. Due to the maturity, economy, and reliability of solving complex problems of finite element software, the finite element method is widely used in solving complex dynamic response problems of pavement structures under moving wheel loads. Some researchers use a simplified two-dimensional finite element model to study the influence of the base crack length and crack inclination angle [5, 6], different pavement materials [7], vehicle speeds, axial loads [8], and other factors on the propagation of reflective cracks. To a certain extent, the two-dimensional pavement model can reflect the propagation mechanism of reflective cracks under environmental load. However, the cracks do not expand uniformly in the road cross section, and the three-dimensional pavement model can better reflect the actual state of the pavement structure.

In order to accurately capture the influence of vehicle loads on crack initiation and propagation, Garzon and Duarte [9] used the finite element method combined with fracture mechanics theory to establish a 3D model of the

airport road and used the method of preset interlayer cracks to predict the cracking of each layer of pavement during use. The results show that the reflective cracks of the airport road are mixed cracks, and the cracks exhibit significant channeling under some loading conditions. Li et al. [10] calculated the fracture factor in pairs formula through experiments and used its predicted value to carry out three-dimensional numerical simulation of reflective cracks in an asphalt overlay of cement concrete pavement. The numerical calculation results of asphalt overlay fatigue are in good agreement with the indoor tests. The degree of crack propagation is often described using the stress intensity factor (SIF), from which researchers can directly understand the cracking process. Elseifi et al. [11] set singular elements at the crack tip and calculated SIF of different contour lines, and the results proved the applicability of the stress intensity factor in 2D and 3D pavement models. Alae et al. [12] established a three-layer three-dimensional model of asphalt pavement with cracks based on the given ambient temperature and vehicle working conditions. The model revealed that the cracks of asphalt pavement are mainly typed I + II fractures. Low-speed driving is more unfavorable to crack propagation. The main disadvantage of cement-stabilized macadam in semirigid base asphalt pavements is fatigue cracking under traffic loads over time [13]. Zhang et al. [14] compared the mechanical response and fatigue damage of semirigid base asphalt pavement structure before and after repairing reflective cracks with polymer by finite element method. Wang and Ma [15] developed an interlayer contact bonding model to simulate the local bonding state between adjacent layers, and using the established semirigid base asphalt pavement structural model, the effect of temperature on the separation area between the asphalt concrete layer and the base was calculated and analyzed. Wang and Yang [16] used the extended finite element method (XFEM) to study the reflection crack mechanism of semirigid asphalt pavement under the combined action of temperature and vehicle load.

In summary, scholars have made many research achievements in the properties of pavement structural materials, the generation of single reflective cracks, and the mechanism of fatigue propagation. However, it is not difficult to find that the influence of multiple reflective cracks on semirigid base asphalt pavement remains to be studied. On the basis of considering the viscoelastic characteristics of asphalt mixtures, this paper examines the dynamic behavior of semirigid pavement structures with multiple reflective cracks under the moving load of vehicles. The research described in this paper focuses on the effects of crack number, crack spacing, and crack length on the stress intensity factor at the tip of reflective cracks and reveals the propagation mechanism of multiple reflective cracks.

2. Methods

2.1. Stress Intensity Factor. Fracture mechanics have been widely used in crack analysis in pavement engineering [17]. Due to the influence of the stress singularity at the crack tip, the stress is difficult to accurately evaluate the working state of the discontinuity problem. Generally, the stress intensity factor is used to describe the crack propagation trend. The reflective cracks in the base layer mainly exhibit open crack and sliding crack propagation behaviors under the action of moving loads. The displacement field near the tip of a reflective crack can be expressed using the following equations:

$$\begin{aligned} u &= \frac{K_{\mathrm{I}}}{4G}\sqrt{\frac{r}{2\pi}}\left[(2\chi-1)\cos\frac{\theta}{2}-\cos\frac{3\theta}{2}\right] \\ &\quad + \frac{K_{\mathrm{II}}}{4G}\sqrt{\frac{r}{2\pi}}\left[(2\chi+3)\sin\frac{\theta}{2}+\sin\frac{3\theta}{2}\right], \\ v &= \frac{K_{\mathrm{I}}}{4G}\sqrt{\frac{r}{2\pi}}\left[(2\chi-1)\sin\frac{\theta}{2}-\sin\frac{3\theta}{2}\right] \\ &\quad - \frac{K_{\mathrm{II}}}{4G}\sqrt{\frac{r}{2\pi}}\left[(2\chi-3)\cos\frac{\theta}{2}+\cos\frac{3\theta}{2}\right], \end{aligned} \tag{1}$$

where G is the shear modulus. u and v are the displacements along the x and y axes, which are functions of time t. In the plane strain state, $\chi = 3 - 4\mu$. r is the distance from the calculation point to the crack tip point. θ is the angle between the polar coordinate system and the line connecting the calculation point and the crack tip point. K_{I} and K_{II} are the stress intensity factors of type I and type II at the crack tip, respectively.

$$\begin{aligned} K_{\mathrm{I}} &= \sqrt{2\pi}\,\frac{G}{1+\chi}\,\frac{|\Delta v|}{\sqrt{r}}, \\ K_{\mathrm{II}} &= \sqrt{2\pi}\,\frac{G}{1+\chi}\,\frac{|\Delta u|}{\sqrt{r}}. \end{aligned} \tag{2}$$

The stress intensity factor at the crack tip can be obtained using the extrapolation method of node displacement. If $(v/\sqrt{r}) = A + Br$, then

$$\begin{aligned} \lim_{r\longrightarrow 0}\frac{v}{\sqrt{r}} &= A, \\ K_{\mathrm{I}} &= \sqrt{2\pi}\,\frac{2GA}{1+\chi}. \end{aligned} \tag{3}$$

Therefore, the stress intensity factor of type I can be derived from the vertical displacement field. The value of K_{II} is obtained in the same way.

The Pook criterion [18] is used to calculate the effective stress intensity factor of composite cracks (I + II), and K_{eff} can be defined using the following equation:

$$K_{\mathrm{eff}} = \frac{0.81K_I + \sqrt{0.45K_I^2 + 3K_{\mathrm{II}}^2}}{1.5}. \tag{4}$$

2.2. Extended Finite Element Method. When the traditional finite element method calculates and simulates the static reflection crack in the semirigid base, it is necessary to use the singular mesh method due to the singularity of the stress at the crack tip. This requires additional nodal processing

and refinement of the elements at the tip of the reflection crack during meshing. A large number of meshes will cause computational difficulties, especially in 3D models. The finite element software ABAQUS provided the Extended Finite Element Method (XFEM) to solve this problem [19]. Based on the idea of unit decomposition, the XFEM adds a jump function to reflect the displacement discontinuity characteristics of the reflective crack region in the pavement structure.

$$\psi(x) = \sum_I N_I(x) q_I \Phi(x) \sum_I N_I(x) = 1, \tag{5}$$

where q_I is a parameter to make the expression reach the conforming approximation. $N_I(x)$ is a jump function, and $\Phi(x)$ is an extended function. The XFEM uses the following equation to simulate cracks:

$$u^k = \sum_I N_I(x) u_I + \sum_J N_J(x) q_J \Phi(x), \tag{6}$$

where q_j is to adjust the function $\Phi(x)$ to achieve the best approximation.

2.3. Crack Fatigue Propagation Theory. The Paris formula is currently the most commonly applied fatigue crack propagation model [20]. After the stress cycle is loaded N times, the crack propagation length is C. Then, the stress is cycled once, and the crack growth is $\Delta C/\Delta N$ (mm/time). Its differential form dC/dN is shown in

$$\frac{dC}{dN} = A(\Delta K)^n. \tag{7}$$

The number of load cycles is obtained by integrating the above equation.

$$N = \frac{1}{A} \int_0^h \frac{1}{(\Delta K)^n} dc, \tag{8}$$

where ΔK is the variation amplitude of the stress intensity factor under a given load. A and n are the fracture parameters of the material, which can be determined experimentally. C is the length of the crack. N is the cumulative fatigue action time of the standard axle load. h is the pavement thickness.

The pavement fatigue life can be calculated by integrating ΔK, where A and n are the key parameters for fracture fatigue analysis.

3. Pavement Simulation Model

In the field of road engineering, the method of finite element numerical analysis is usually used to study the mechanical characteristics of reflection cracks. In this section, based on ABAQUS finite element software and XFEFM module, a subroutine for realizing moving load is written, and the effect of horizontal friction between tire and road surface is considered, and the cracking mechanism of multiple reflective cracks in semirigid pavement structure under traffic load is analyzed.

3.1. Model Description. The pavement model's length, width, and height are 6m, 6m, and 4m [21]. The pavement structure consists of six layers: SBS-AC13, SBS-AC20, A70-AC25, cement-stabilized base, cement-stabilized subbase, and natural soil, as shown in Figure 1(a). Figure 1(b) is the midsection of the road model along the Z axis. There are two reflective cracks in the pavement structure. A reflective crack transversely penetrates the base along the Y axis, and there is a parallel reflective crack not penetrating the base on the left.

The material parameters of semirigid base asphalt pavement structures are shown in Table 1. The asphalt mixture has obvious viscoelasticity, while the remaining layers are calculated as linear elastic materials. The viscoelastic characteristics of asphalt mixtures are described by the generalized Maxwell model in the present paper, which is composed of n parallel Maxwell elements and a linear elastic spring element in parallel. The stress relaxation modulus at reference temperature $T0$ is

$$E(T_0, t) = E_e + \sum_{i=1}^{n} E_i \exp\left(-\frac{t}{\tau_i}\right), \tag{9}$$

where E_e is the elastic modulus of the spring element. E_i and τ_i are the elastic modulus and relaxation time of the i th Maxwell Table 2model spring, respectively. The Prony parameters in ABAQUS finite element software are consistent with the mathematical expression of (9); hence, it can commendably express the viscoelastic properties of the asphalt mixture. Table 1 shows the Prony parameters of the asphalt layer at 20 ˚C [22].

3.2. Basic Assumptions and Boundary Conditions. When calculating the pavement structure model, it is necessary to make the following assumptions about the pavement model materials and boundary conditions: (1) the pavement structure is an infinite system of half-space; (2) the materials of each structural layer are homogeneous and isotropic; (3) displacement between layers is continuous; (4) stress, strain, and displacement are all zero in infinite depth of soil; (5) there is no displacement at the bottom of pavement model, and the displacements of the x-axis and the z-axis of the transverse and longitudinal sides, respectively, are constrained to be zero.

The bottom surface of the pavement model is completely fixed ($U1$=U2=$U3 = 0$, UR1 = UR2 = UR3 = 0). The two sides of the model perpendicular to the Z axis limit the displacement in the Z direction and the rotation in the XY direction ($U3 = 0$, UR1 = UR2 = 0), and the two sides perpendicular to the x-axis limit the displacement in the X direction and the rotation in the YZ direction ($U1 = 0$, UR2 = UR3 = 0).

3.3. Moving Traffic Load Setting and Mesh Division. The movement of the load is realized using the ABAQUS software user subroutine. The DLOAD and UTRACLOAD subroutines specify the variation of the amplitude of the distributed load (F) as a function of time (TIME*) in a specific coordinate system (COORDS*). UTRACLOAD

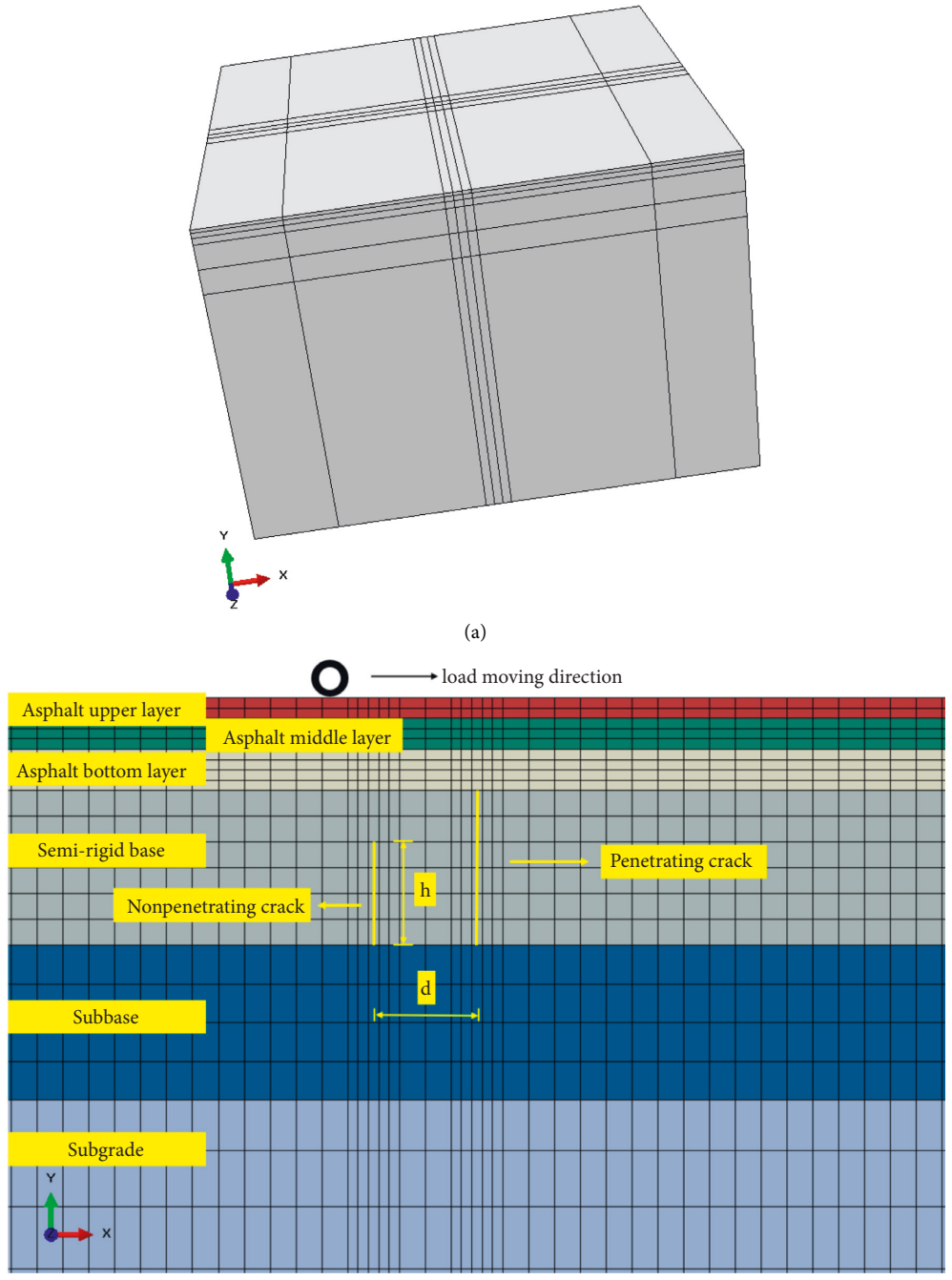

Figure 1: Pavement model. (a) Overall structure diagram of semirigid base asphalt pavement. (b) Mid-section along the Z axis.

Table 1: Properties of layers.

Layer	Material	Young's modulus (MPa)	Poisson's ratio	Thickness (cm)
Asphalt concrete upper layer	SBS-AC13	-	0.35	4
Asphalt concrete middle layer	SBS-AC20	-	0.35	6
Asphalt concrete bottom layer	A70-AC25	-	0.35	8
Semirigid base	Cement-stabilized macadam	1500	0.25	30
Subbase	Cement-stabilized gravel	1300	0.3	30
Subgrade	Compacted soil	250	0.35	-

Table 2: Prony parameters of each asphalt mixture.

Relaxation time τ_i/s	Relative shear modulus g_i		
	SBS-AC13 (Instantaneous modulus 1550 MPa)	SBS-AC20 (Instantaneous modulus 1250 MPa)	A70-AC25 (Instantaneous modulus 2450 MPa)
0.00001	0.31288	0.42854	0.34127
0.0001	0.20212	0.18515	0.20200
0.001	0.21377	0.17640	0.21428
0.01	0.14498	0.11444	0.14543
0.1	0.06803	0.05524	0.06354
1	0.02679	0.02179	0.02084
10	0.01078	0.00858	0.00674
100	0.00428	0.00328	0.00224
1000	0.00264	0.00204	0.00121

Note. Asphalt material parameters are taken at 20 ˚C.

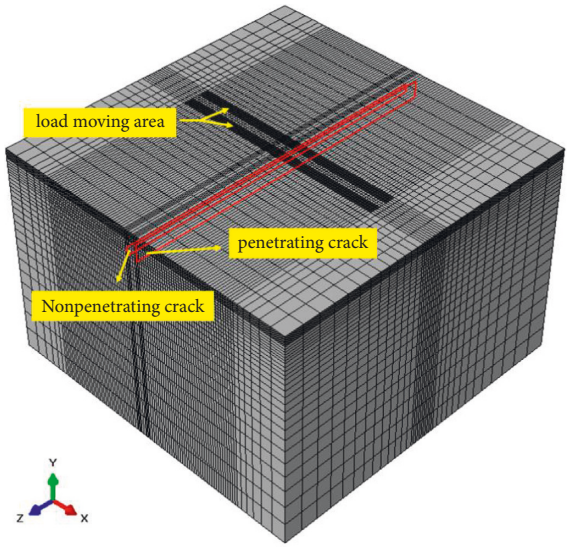

Figure 2: Finite element mesh of the pavement structure.

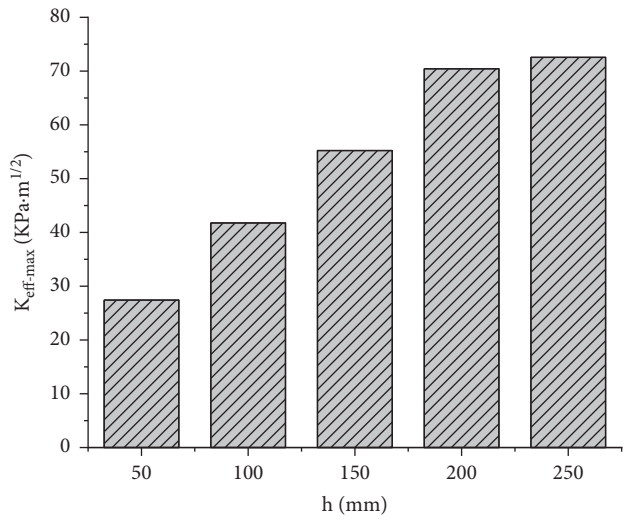

Figure 3: Keff-max of single nonpenetrating crack time history curve with various lengths.

needs to additionally specify the direction of shear stress by using the vector (T_USER*). The relevant Chinese regulations stipulate that the design of asphalt pavement adopts a single-axle-two-wheel set axle load with an axle load of 100 kN (BZZ-100) as the design axle load. When the vehicle is parked on the road surface, the pressure on the contact area of the road surface is 0.7 MPa. At the same time, considering the influence of horizontal force, the rolling friction coefficient is taken as 0.05; that is, the horizontal friction force is 0.035 MPa, and the load direction is opposite to the driving direction. According to the relevant research [23], the shape of the tire ground contact is close to a rectangle with the increasing of axle load. The traffic load area is set up as two parallel rectangular areas with a length of 4 m, a width of 0.192 m, and a spacing of 0.134 m. The simulated vehicle load moves at a speed of 80 km/h in this area.

To increase the calculation accuracy of the model, a relatively fine mesh size was adopted along the truck wheel path, where the stresses and displacement are higher. As seen in Figure 2, the dense mesh was used near the reflective crack and load moving area, while a relatively coarse mesh size was adopted far away from the loading area. C3D8R was selected as the grid type, and the total number of finite elements after meshing is 206232.

For the mechanical behavior inside the pavement structure under vehicle loads, there is a superimposed interference effect between the cracks when the two cracks are close to each other. The effect will gradually decrease with the distance between the cracks increasing. In this paper, the effect of horizontal crack spacing and nonpenetrating reflective crack height on the propagation of multiple reflective cracks structure of semirigid pavement is studied.

4. Results and Discussion

4.1. Effect of Length (h) on Single Nonpenetrating Crack Propagation. First, the dynamic response of pavement with single nonpenetrating reflective cracks under moving loads is calculated. Figure 3 shows the peak value of the effective stress intensity factor (Keff-max) for nonpenetrating cracks with different lengths. It can be seen from Figure 3 that the

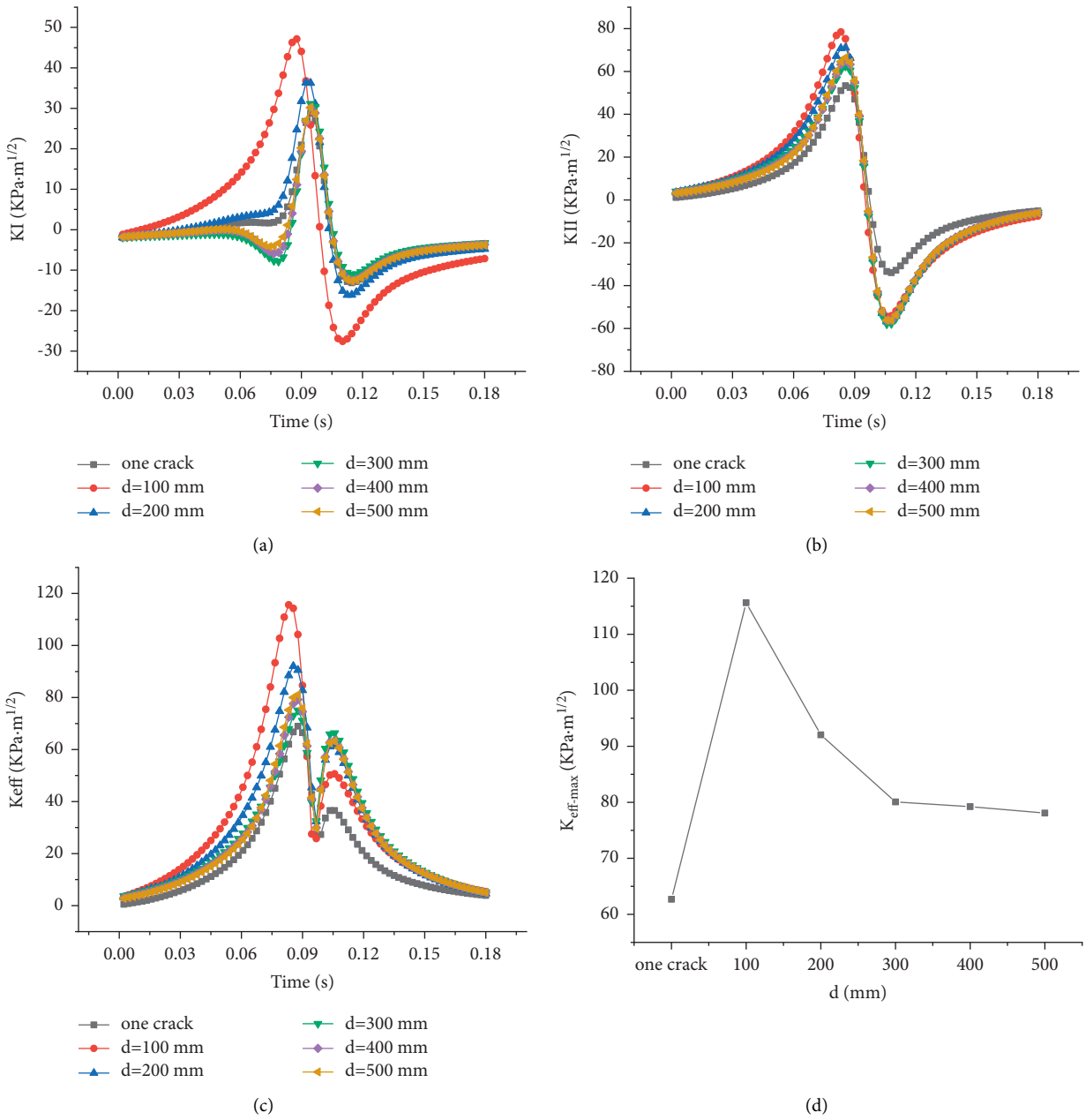

Figure 4: The SIF of the penetrating crack time history curve with various spacings. (a) KI; (b) KII; (c) Keff; (d) Keff-max.

peak value of the effective stress intensity factor increases with the increase of crack length. When the crack length is 250 mm, the Keff peak value increases by 161.03% compared with 50 mm.

4.2. Effect of Spacing (d) on Multiple Crack Propagation. In this section, the y-direction length of the nonpenetrating reflective crack is 25 cm. The effect of crack spacing on the stress intensity factor of multicrack pavement structures is studied by changing the horizontal distance between two reflective cracks ($d = 0$, 100, 200, 300, 400, 500 mm), in which $d = 0$ means that there is only one reflection crack through the base layer.

4.2.1. Effect on Penetrating Crack. Figure 4 presents the stress intensity factors of penetrating crack time history curves with various spacings. It can be seen from Figure 4(a) that the interference effect between the two cracks is more evident when the crack spacing is 100 mm and 200 mm. As the load moves to the plane where the crack is located, KI of the through crack is a positive value, and the through crack has a trend of type I expansion at this time. Except for the crack spacing of 100 mm and 200 mm, the value of KI is negative. The fracture surfaces are pressed against each other, and there is no crack growth of type I. The value of KI reaches a positive peak as the load moves along the x-axis near the top of the crack. It is not difficult to know that as the horizontal distance of the fracture gets closer, the peak value

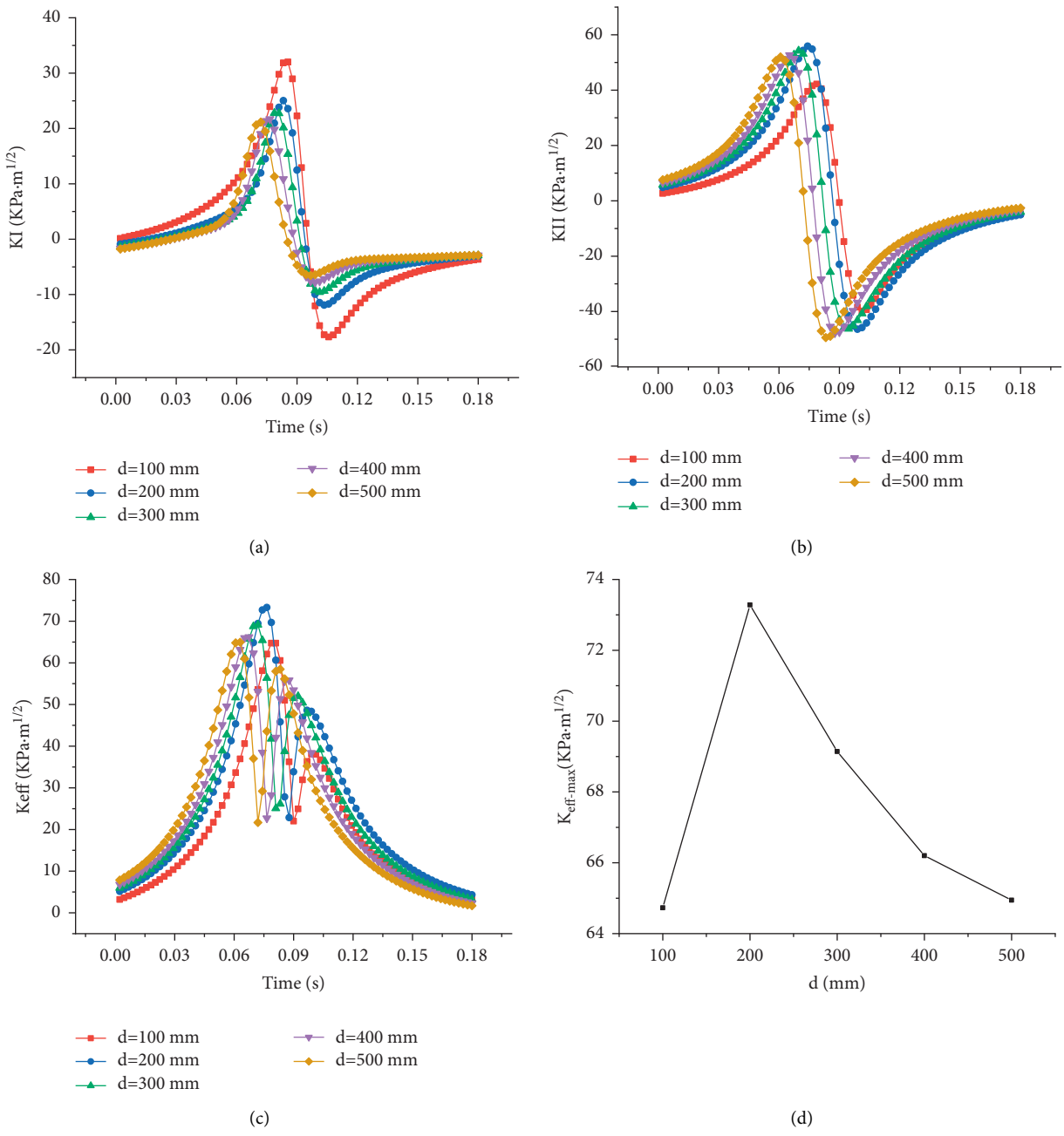

Figure 5: The SIF of nonpenetrating crack time history curve with various spacings. (a) KI; (b) KII; (c) Keff; (d) Keff-max.

is more considerable, and the time point of reaching the peak value is also earlier. Over time, the moving load will move away from the reflective crack. The value of KI decreased to a negative peak and then gradually increased and approached 0.

Figure 4(b) shows the stress intensity factor of the shear mode time history curve. As the load moves across the upper part of the penetrating crack, the value of KII gradually increases to a positive peak. The shear direction changes, and KII decreases to a negative peak value after the moving load passes through the plane of the reflective crack. Overall, the value of KII decreases with the increase of fracture spacing.

The effective stress intensity factor, calculated by the Pook criterion, is convenient to investigate the comprehensive expansion of the penetrating crack at different spacing. It can be observed in Figure 4(c) that the Keff time history curve as a whole presents a "saddle shape." Keff reaches the peak value before the moving load passes by the plane where the reflective crack is located. Reflective cracks exist in the form of opening and shear failure. Under the action of friction and shear on the road surface, Keff gradually decreases with time and then suddenly increases to the subpeak value. The cracks exhibit shear failure due to the closure of the cracks under compression. Compared with a single penetrating reflective crack, increasing the number of

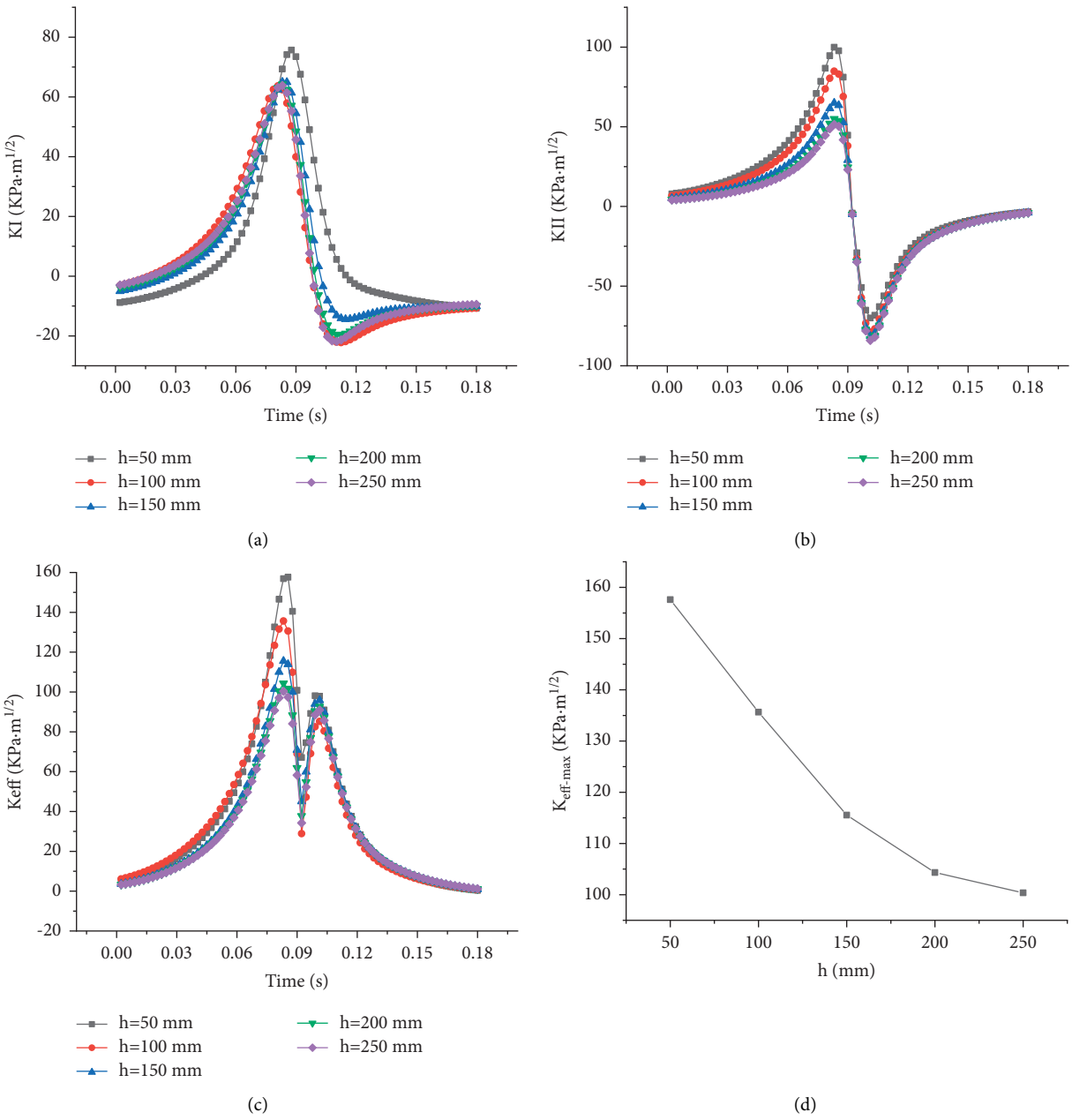

Figure 6: The SIF of nonpenetrating crack time history curve with various lengths. (a) KI; (b) KII; (c) Keff; (d) Keff-max.

cracks in asphalt pavement structure will significantly improve the Keff value of penetrating cracks. As shown in Figure 4(d), the Keff peak value generally indicates a decreasing trend with the increase of the crack spacing. The Keff-max value at the crack spacing of 100 mm increases by 67.70% compared with the single penetrating crack. The effect of crack spacing on the Keff peak value gradually weakened after the crack spacing was increased to 300 mm. The Keff-max when the crack spacing is 500 mm only increases by 13.25%. What is more, it can be observed that the stress intensity factor under shear failure condition, in general, is more significant than that under opening failure. Therefore, shear failure is the main reason for the appearance of reflective cracks in the pavement.

4.2.2. Effect on Nonpenetrating Crack. Figure 5 presents the stress intensity factors of the nonpenetrating crack time history curve with various spacings. As the load moves over the asphalt pavement, the value of KI first increases rapidly to decrease to a negative peak and approaches 0 smoothly. As the load moves to the reflective crack, the value of KI is a positive value under the action of friction force and pressure, and the crack is in an opening mode expansion state. The value of KI changes from positive to negative after the load passes by the plane where the reflective crack is located. The horizontal friction closes the crack as it causes the crack surface to be squeezed.

Similar to Figure 4(b), Figure 5(b) shows that the value of KII first gradually increased to a positive peak, then rapidly

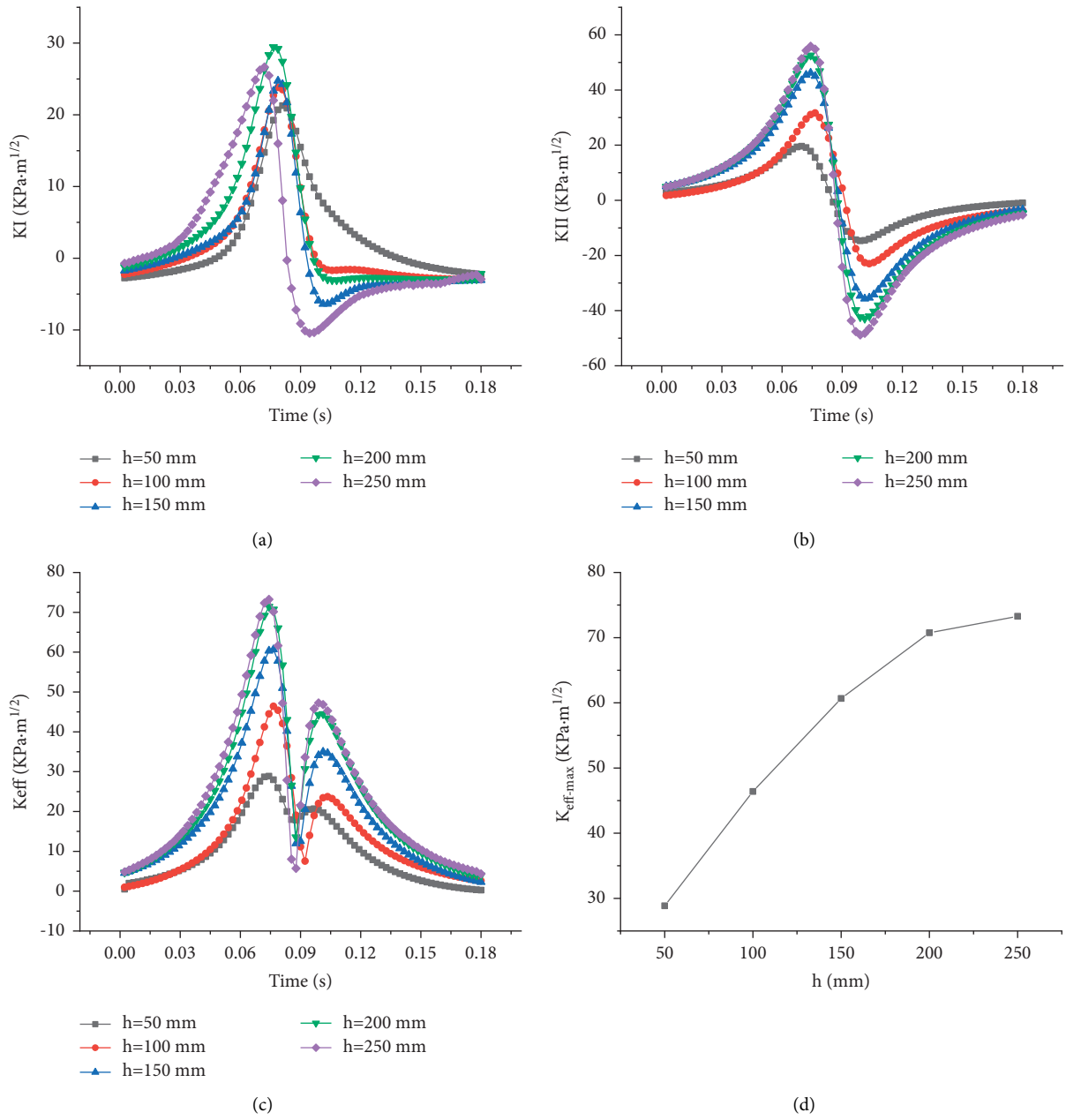

Figure 7: The SIF of nonpenetrating crack time history curve with various lengths. (a) KI; (b) KII; (c) Keff; (d) Keff-max.

decreased to a negative peak, and finally tended to level off. The change in the direction of shear stress at the tip of the reflective crack causes positive and negative changes in KII. Similar to penetrating cracks, the stress intensity factor of shear mode is larger than that in an open way.

Figure 5(c) and Figure 5(d) show the Keff time history curve and its peak value of the nonpenetrating crack, respectively. As seen in Figure 5, the peak value of Keff first increases slowly and subsequently decreases with the change of the crack spacing. The reason for the small Keff peak in the crack spacing of 100 mm may be that the penetrating crack over the nonpenetrating crack will bear more stress as the two cracks are closer together. The Keff peak value at a crack spacing of 200 mm reaches the maximum, which also means that the unpenetrated cracks are most likely to grow upward at this time. When the crack spacing is greater than 300 mm, the influence of crack spacing on the peak value of Keff gradually diminishes. Compared with the data in Figure 4(d), it can be seen that the crack spacing has a greater impact on the penetrating crack.

4.3. Effect of Length (h) on Multiple Crack Propagation. In this section, the horizontal spacing between two reflective cracks is 20 cm. A series of models with different cracking lengths of nonpenetrating cracks are performed. The influence of nonpenetrating crack length ($h = 50$, 100, 150, 200, 250 mm) on the propagation of multiple reflective cracks in asphalt pavement structures is analyzed.

Table 3: Keff-max fitting polynomial and fracture life.

Condition	$K_{\text{eff-max}}$ fitting Polynomial	R2	N
Presence of penetrating crack	$K_{\text{eff-max}} = 40.319C^3 - 26.452C^2 + 7.1793C + 0.0149$	0.993	4.658×107
No penetrating crack	$K_{\text{eff-max}} = -15.165C^3 + 1.7541C^2 + 3.0475C + 0.1161$	0.991	2.475×107

4.3.1. Effect on Penetrating Crack. Figure 6 presents the stress intensity factors of the penetrating crack time history curve with various lengths of nonpenetrating cracks. As shown in Figure 6(a), the KI value of the penetrating crack is the largest when the length of the nonpenetrating crack is 50 mm. As the length of the nonpenetrating crack increases, the KI time-history curves of the penetration crack are basically consistent. At this time, the various sizes of the nonpenetrating crack have little effect on the open-mode propagation of the penetrating crack. Figure 6(b) shows that the length of the unpenetrated crack has a noticeable effect on the KII value of the penetrating crack before the load moves to the plane where the crack is located. This is due to the presence of unpenetrated reflective cracks in the area. It can be observed from Figure 6(c) that the length of the unpenetrated fracture has a significant effect on the peak value of the effective stress factor of the penetration fracture, especially in the first 0.09 seconds. Owing to the larger values of KI and KII, the Keff peak value is larger than that of the other models, and the tendency of crack propagation and failure is obvious. The peak value of Keff showed a decreasing trend when the unpenetrated crack length increased from 50 mm to 250 mm, and the decreasing rate gradually slowed down. This indicates that when a micro-crack is just initiated beside the reflection crack that penetrates the base layer, the penetrating crack will share more vehicle load, and its cracking speed is faster.

4.3.2. Effect on Nonpenetrating Crack. Figure 7 illustrates the stress intensity factors of the nonpenetrating crack time history curve with various lengths. The KII time history curve of the type II stress intensity factor of the unpenetrated fracture is similar to that in Figure 6(b). However, the difference is that the KII negative peak value of the nonpenetrating crack also decreases to a certain extent. From Figure 7(c) and Figure 7(d), it can be seen that the peak value of the stress intensity factor of nonpenetrating crack increases with the increasing length, but the increase rate decreases continuously. In summary, the cracks first dehisce from the bottom of the base layer in a semirigid asphalt pavement structure. The cracks spread to the asphalt pavement layer under the action of the vehicle load, and the cracking speed gradually accelerated.

4.4. Fracture Life of Nonpenetrating Cracks. The fracture life of the asphalt pavement structure was calculated based on the Pairs formula. The values of A and n in (10) are taken as 10–6.92 and 4, respectively [24]. In this paper, the fracture life, which is the extension of the nonpenetrating crack from the initial depth to the whole base layer under moving load, was calculated assuming that the base layer fracture initial length was 5 cm.

The Keff data of nonpenetrating reflective cracks at different depths in Figures 3 and 7(d) are fitted using the following formula:

$$K_{\text{eff-max}} = \xi_1 C^3 + \xi_2 C^2 + \xi_3 C + \xi_4, \quad (10)$$

where ξ is the fitting coefficient of polynomial. C is the length of reflective crack. The fracture life can be calculated by substituting the fitting polynomial into Equation (10). The fitted polynomial of the peak value of the effective stress intensity factor of the unpenetrated crack at different depths and its fracture life is shown in Table 3.

It can be seen from Table 3 that the fatigue life of nonpenetrating reflective cracks extending from 5 cm in length to penetrating the entire base layer when there is a penetrating crack is reduced by 46.87%. Due to the interference effect among multiple cracks, the service life of the semirigid pavement with multiple reflective cracks will be significantly shortened.

5. Conclusions

It is widely known that crack prevention and control is a long-term research field of road engineering. A correct understanding of the propagation mechanism between cracks will help road researchers make correct design and treatment decisions. In this study, the FEM software ABAQUS was used to establish a 3D asphalt pavement model. The propagation behavior of multiple reflective cracks in the semirigid pavement is studied using the Extended Finite Element Method and fatigue fracture theory. Based on the simulation results, the following conclusions can be drawn:

(1) Reflective cracks in semirigid pavement are composite cracks of type I and type II under the action of moving load. The value of KI is larger than that of KII in both the single-cracked structure and the double-cracked structure, indicating that shear cracking is the main reason for the propagation of reflective cracks. With regard to a single crack, the SIF in multiple crack structures increases significantly. An increase in the number of reflective cracks will accelerate crack propagation and pavement damage.

(2) Assuming that the length of the nonpenetrating crack is constant, the increase in crack spacing will gradually reduce the growth rate of penetrating cracks, while the growth rate of nonpenetrating cracks shows a trend of first increasing and then decreasing with the increasing of crack spacing. According to the Keff peak value distribution, the

reflective crack spacing has a more significant influence on the penetrating crack.

(3) Assuming that the crack spacing is constant, the growth rates of the nonpenetrating crack in both the single crack pavement model and the multiple crack pavement model all accelerate with the increasing of the fracture length, but the increasing range decreases continuously. The propagation of a penetrating crack is less affected by the length of the nonpenetrating crack. In conclusion, the growth rate of unpenetrated cracks in the base layer increases as they propagate towards the surface layer.

(4) Based on the Pairs formula, the fatigue failure life of unpenetrated reflective cracks with an initial length of 5 cm was calculated and analyzed. The fracture life of the semirigid base in the multiple crack pavement structure is reduced by 46.87% compared with the base containing only nonpenetrating reflective cracks. It can be seen that the service life of the asphalt pavement structure will be severely shortened by the appearance of multiple reflective cracks. Therefore, attention should be given to the prevention and control of reflective cracks in the early initiation stage. For example, the location of the crack is identified by ground-penetrating radar at first. Afterward, the reflective cracks are eliminated by methods such as polymer grouting.

Data Availability

All data included in this study are available from the corresponding author upon request.

Conflicts of Interest

The authors declare that they have no conflicts of interest.

References

[1] J. Gajewski and T. Sadowski, "Sensitivity analysis of crack propagation in pavement bituminous layered structures using a hybrid system integrating artificial neural networks and finite element method," *Computational Materials Science*, vol. 82, pp. 114–117, 2014.

[2] Q. Yue, H. Xiao, and J. Zou, "Analysis of stress and displacement field in flexible layered pavement based on boundary element method," *Journal of Highway and Transportation Research and Development*, vol. 5, no. 1, pp. 19–23, 2011.

[3] Y. Miao, T. He, Q. Yang, and J. Zheng, "Multi-domain hybrid boundary node method for evaluating top-down crack in Asphalt pavements," *Engineering Analysis with Boundary Elements*, vol. 34, no. 9, pp. 755–760, 2010.

[4] Z. Tang, F. Huang, and H. Peng, "Mode I fracture behaviors between cement concrete and asphalt concrete layer," *Advances in Civil Engineering*, vol. 2021, Article ID 6658023, 11 pages, 2021.

[5] X. Wang, K. Li, Y. Zhong, Q. Xu, and C. Li, "XFEM simulation of reflective crack in asphalt pavement structure under cyclic temperature," *Construction and Building Materials*, vol. 189, pp. 1035–1044, 2018.

[6] L. Ann Myers, R. Roque, B. Birgisson, and B. Birgisson, "Propagation mechanisms for surface-initiated longitudinal wheelpath cracks," *Transportation Research Record: Journal of the Transportation Research Board*, vol. 1778, no. 1, pp. 113–122, 2001.

[7] J. Wei, J. Shi, and J. Liang, "Overlay test to investigate the crack propagation of a large-size asphalt mixture," *Journal of Materials in Civil Engineering*, vol. 32, no. 5, Article ID 04020097, 2020.

[8] H. Wang, Y. Wu, J. Yang, and H. Wang, "Numerical simulation on reflective cracking behavior of asphalt pavement," *Applied Sciences*, vol. 11, p. 7990, 2021.

[9] J. Garzon, C. A. Duarte, and W. Buttlar, "Analysis of reflective cracks in airfield pavements using a 3-D generalized finite element method," *Road Materials and Pavement Design*, vol. 11, no. 2, pp. 459–477, 2010.

[10] Q. Li, Z. Chen, S. Luo, and R. Ince, "Reflection crack analysis of asphalt overlay on cement concrete pavement based on XFEM," *Advances in Civil Engineering*, vol. 2021, Article ID 1230447, 10 pages, 2021.

[11] M. A. Elseifi, J. Baek, and N. Dhakal, "Review of modelling crack initiation and propagation in flexible pavements using the finite element method," *International Journal of Pavement Engineering*, vol. 19, no. 3, pp. 251–263, 2018.

[12] M. Alae, M. Ling, H. F. Haghshenas, and Y. Zhao, "Three-dimensional finite element analysis of top-down crack propagation in asphalt pavements," *Engineering Fracture Mechanics*, vol. 248, Article ID 107736, 2021.

[13] Y. Liu, P. Su, M. Li, Z. You, and M. Zhao, "Review on evolution and evaluation of asphalt pavement structures and materials," *Journal of Traffic and Transportation Engineering*, vol. 7, no. 5, pp. 573–599, 2020.

[14] B. Zhang, X. Zhang, Y. Zhong et al., "Research on fatigue model of semi-rigid base asphalt pavement before and after polymer grouting," *Advances in Civil Engineering*, vol. 2021, Article ID 6658943, 16 pages, 2021.

[15] X. Wang and X. Ma, "Responses of semi-rigid base asphalt pavement with interlayer contact bonding model," *Advances in Civil Engineering*, vol. 2020, Article ID 8841139, 13 pages, 2020.

[16] X. Wang and Y. Zhong, "Reflective crack in semi-rigid base asphalt pavement under temperature-traffic coupled dynamics using XFEM," *Construction and Building Materials*, vol. 214, pp. 280–289, 2019.

[17] D. Ramsamooj, G. Lin, and J. Ramadan, "Stresses at joints and cracks in highway and airport pavements," *Engineering Fracture Mechanics*, vol. 60, no. 5-6, pp. 507–518, 1998.

[18] Q. F. Li, L. Zhu, G. Jin, and X. F. Cui, "3D-Modeling and numerical analysis of fracture behavior in AFM-specimen on mixed-mode I-II loading condition," *Advanced Materials Research*, vol. 450-451, pp. 1391–1394, 2012.

[19] L. Wen and R. Tian, "Improved XFEM: a," *Computer Methods in Applied Mechanics and Engineering*, vol. 308, pp. 256–285, 2016.

[20] A. A. Abdulshafi and K. Majidzadeh, "J-integral and cyclic plasticity approach to fatigue and fracture of asphaltic mixtures," *Transportation Research Record*, vol. 1034, pp. 112–123, 1985.

[21] Y. Deng, X. Luo, F. Gu, Y. Zhang, and R. L. Lytton, "3D simulation of deflection basin of pavements under high-speed moving loads," *Construction and Building Materials*, vol. 226, pp. 868–878, 2019.

[22] O. C. Assogba, Y. Tan, X. Zhou, C. Zhang, and J. N. Anato, "Numerical investigation of the mechanical response of semi-

rigid base asphalt pavement under traffic load and nonlinear temperature gradient effect," *Construction and Building Materials*, vol. 235, Article ID 117406, 2020.

[23] X. Sui and L. Cao, X. Ma, H. Wang, and Z. Dong, Research on transversely isotropic permeability of asphalt pavement: l," *Construction and Building Materials*, vol. 251, Article ID 118958, 2020.

[24] P. Liu, J. Chen, G. Lu, D. Wang, M. Oeser, and S. Leischner, "Numerical simulation of crack propagation in flexible asphalt pavements based on cohesive zone model developed from asphalt mixtures," *Materials*, vol. 12, no. 8, 8 pages, Article ID 1278, 2019.